Modeling of Poly(ADP-ribose)polymerase (PARP) Inhibitors. Docking of Ligands and Quantitative Structure−Activity Relationship Analysis

Gabriele Costantino, Antonio Macchiarulo, Emidio Camaioni, and Roberto Pellicciari*

Dipartimento di Chimica e Tecnologia del Farmaco, Università di Perugia, Via del Liceo 1, 06127 Perugia, Italy

Received March 15, 2001

Poly(ADP-ribose)polymerase-1 (PARP-1) is a nuclear enzyme that has recently emerged as an important player in the mechanisms leading to postischemic neuronal death, and PARP inhibitors have been proposed as potential neuroprotective agents. With the aim of clarifying the structural basis responsible for PARP inhibition, we carried out a computational study on 46 inhibitors available through the literature. Our computational approach is composed of three parts. In the first one, representative PARP inhibitors have been docked into the crystallographic structure of the catalytic domain of PARP by using the Autodock 2.4 program. The docking studies thus carried out have provided an alignment scheme that has been instrumental for superimposing all the remaining inhibitors. Upon the basis of this alignment scheme, a quantitative structure−activity relationship (QSAR) analysis has been carried out after electrostatic and steric interaction energies have been computed with the RECEPTOR program. The QSAR analysis yielded a predictive model able to explain much of the variance of the 46-compound data set. The inspection of the QSAR coefficients revealed that the major driving force for potent inhibition is given by the extension of the contact surface between enzyme and inhibitors while electrostatic energy and hydrogen bonding capability play a minor role. Finally, the projection of the QSAR coefficients back onto the X-ray structure of the catalytic domain of PARP provides insights into the role played by specific amino acid residues. This information will be useful to address the design of new selective and potent PARP inhibitors.

Introduction

Poly(ADP-ribose)polymerase-1 (PARP-1) is a chromatin-bound nuclear enzyme involved in a variety of physiological functions related to genomic repairs, including DNA replication and repair, cellular proliferation and differentiation, and apoptosis.[1] PARP, selectively activated by DNA strand breaks, uses nicotinamide dinucleotide (NAD) as substrate and catalyzes the poly-ADP ribosilation of a variety of proteins, including caspases, topoisomerases, histones, and PARP itself.[2]

Because of its involvement in processes related to DNA damages, PARP has been considered for several years as a suitable target for antitumoral drugs.[3] Recent evidences, however, including the availability of knockout mice,[4] demonstrate that inhibition of PARP may have a great impact in the protection from neuronal lesions after cerebral ischemia.[5−9] Indeed, many of the strategies so far pursued to reduce neuronal damage and death following cerebral ischemia have been based on the modulation of membrane glutamate receptors, either ionotropic receptors or metabotropic receptors, but much of the therapeutic expectance reposed on glutamate modulators has largely been unmet in a clinically useful way.[10] There is indeed an emerging awareness that the blockade of calcium overload, mediated by glutamate receptors, which follows the excitotoxic stimulus, is not sufficient to protect against neuronal degeneration and that other cellular mechanisms should also be targeted for the rational design of new therapeutic entities.[11] A variety of evidences gathered over the past few years indicate the production of intracellular free radical species as the principal cause of neuronal death after cerebral ischemia.[12] Free radical species, among which NO and peroxynitrite play a pivotal role, disrupt a variety of structural and metabolic cellular elements and elicit DNA damage. The DNA strand breaks provoked by free radical species activate PARP, which catalyzes the transfer and polymerization of units of ADP-ribose from NAD to target proteins. This causes a quick depletion in the cellular reservoir of NAD which in turn results in a diminished ATP production. In an attempt to resynthesize NAD, the cell further consumes ATP, which results in energy crisis and, ultimately, in cell death. According to this paradigm, selective inhibitors of PARP-1 may play an important role as potential neuroprotective agents and may have therapeutic application in a variety of neurological diseases related to excitotoxic insults.[13−15]

Most of the PARP inhibitors so far developed are structural analogues of NAD and are thought to compete with NAD itself at the level of the catalytic domain. Simple chemical modifications of the nicotinamide moiety afforded competitive PARP inhibitors, which were, however, characterized by a low potency and a poor selectivity. Benzamide derivatives (Chart 1, **I**) were shown to be inhibitors of PARP in the low micromolar range, and 3-substitution with electron-donating groups generally increases the potency.[16] The synthesis of conformationally constrained cyclic derivatives of benzamide, such as 5- or 7-substituted dihydroisoquinolin-1-ones (**II, III**) has allowed demonstration of a confor-

* To whom correspondence should be addressed. Tel: ++39 075 585 5120. Fax: ++39 075 585 5124. E-mail: rp@unipg.it.

10.1021/jm010116l CCC: $20.00
Published on Web 10/13/2001

Chart 1

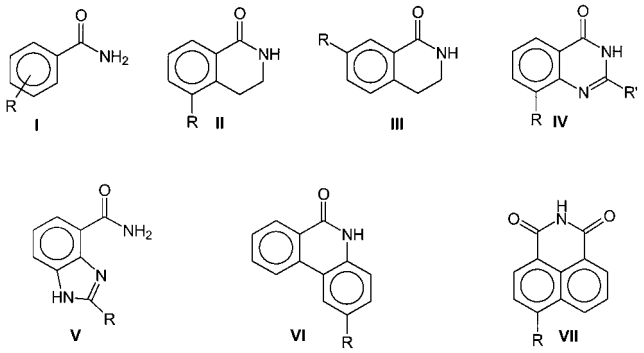

mational requirement for an anti disposition of the amide moiety.[17] Other cyclic derivatives of benzamide have been reported as PARP inhibitors, including 2,8-substituted quinazolin-4-ones (**IV**),[16,18] benzimidazoles (**V**),[19] lactames such as phenantidrione (**VI**),[16] and 1,8-naphthalamides (**VII**),[16] with an increased potency with respect to benzamides. Structural elaboration of 5-substituted isoquinolin-1-ones has led to the synthesis of DPQ (**18**, Table 1), the most potent inhibitor of PARP so far known.[9] The analysis of the available benzamide-related PARP inhibitors has allowed the drawing of a consensus pharmacophore, constituted by an anti arylamide moiety and at least one aromatic ring with substituents in the 3-position of the benzamide nucleus increasing the potencyand substituents in 2-, 4-, or 5-positions being deleterious for the activity.

The availability of crystallographic structures of the catalytic fragment of PARP, also complexed with competitive inhibitors, has allowed the above SAR scheme to be rationalized on a structural basis.[20−22] Indeed, in all the PARP-inhibitor complexes so far available, the amide moiety of the inhibitor invariably interacts with the backbone atoms of Gly863, while the aromatic portion interacts, presumably through $\pi-\pi$ interactions, with Tyr907 (Figure 1).

Nevertheless, the variability in potency found in PARP inhibitors (50% inhibitory concentrations (IC_{50}s) ranging from submicromolar to high-micromolar values for structurally related molecules) suggests that accessory binding pockets in the enzyme active site must be present and play a pivotal, still unclarified, role in determining the affinity. It is therefore conceivable that the identification of such areas can be exploited for the design of novel, more potent PARP-1 inhibitors. Also in view of the potential therapeutic importance that PARP inhibitors may have in a variety of CNS, vascular, and inflammatory diseases, we engaged ourselves in a program devoted to the design and synthesis of novel, selective PARP inhibitors. In this frame, we report here a molecular modeling study aimed at mapping the topography of the active site of PARP-1 and at identifying the structural requirement for PARP inhibition. A total of 46 PARP inhibitors for which homogeneous biological values are available were collected from the literature and reported in Table 1 along with their inhibitory IC_{50} values.

The methodological approach employed for this purpose is composed of three steps. In the first one, a docking analysis was conducted on a small subset of representative PARP inhibitors to define the orientation of inhibitors inside the binding pockets and to propose a superimposition scheme for the remaining inhibitors; then, surface maps of the physicochemical properties of the catalytic site of PARP-1 were generated by using the RECEPTOR approach (see Methods). A quantitative structure−activity relationship (QSAR) analysis was finally carried out on the chosen inhibitors to study the dependence of their inhibitory activity on a set of structural and energetic descriptors related to the binding energy and calculated from the above maps. The thus obtained information is projected back into the crystallographically determined binding pocket of PARP-1 to highlight those residues most relevant for high-affinity binding.

Methods

All compounds were constructed starting from fragment dictionary and geometry optimized using the consistent valence force field (CVFF 95)[23] with the Smart Minimizer protocol of Open Force Field (OFF). Atomic charges were computed using the semiempirical MOPAC /AM1 method. The simulated annealing algorithm of Autodock 2.4 program was used for docking experiments. Details about the methodology used by Autodock are described elsewhere.[24]

The region of interest used by Autodock was defined in such a way to include a large portion of the catalytic site of PARP (Tyr710, Gln763, Asp766−Asn767, Asp770, Trp861−Ser864, Arg878−Ala880, Gly888−Met890, Gly894, Tyr896−Ala898, Lys903−Ser904, Tyr907, Asn987−Tyr989). In particular, a grid of 80 points in *x*, *y*, and *z* directions was built centered on the center of mass of the above portion of the catalytic site of PARP. A grid spacing of 0.375 and a distance dependent dielectric function were used for the calculation of the energetic maps.

All docked compounds were subjected to 10 runs of Autodock search. Each run was composed of 500 cycles of simulated annealing and 30 000 steps of accepted/rejected configurations. The default values of all other parameters were used. A cluster analysis was performed on the results from the 10 runs using a root mean square (rms) tolerance of 0.5 Å.

The alignment between docked and undocked compounds was performed by manually fitting the atomic coordinates of groups involved in the conserved interaction (oxygen and nitrogen of the amide moiety, centroid of the phenyl group of the isoquinoline moiety, Figure 3). Where possible also, the atomic coordinates of groups involved in nonconserved interactions were fitted.

The RECEPTOR module of Cerius2 was used to build binding site surfaces of the catalytic domain of PARP.[25,26] Briefly, these surface models represent the essential features of the binding site by assuming complementarity between the shape and properties of the binding site of a receptor or enzyme and a set of inhibitors. Three-dimensional (3D) surfaces of the binding site enclose the most active members (after appropriate alignment) of the starting set of compounds. Note that errors in alignment can lead to incorrect, poorly predictive receptor surface models. This problem was overcome by using information obtained from docking experiments. The surface is generated from a "shape field". The atomic coordinates of the contributing models are used to compute field values on each point of a 3D grid using a van der Waals function (eq 1):

$$V(r) = r - \mathrm{VdWr} \qquad (1)$$

where *r* is the distance from the atomic coordinate to the grid point (called *surface fit* and set here to 0.1) and VDWr is the van der Waals radius of the atom.

The contribution of compounds for surface generation was weighted taking into account their respective activity. The interaction energies were calculated after all molecules inside the surface were minimized to maximize their complementa-

Table 1. Inhibitory Values (IC_{50}s) of Selected Classes of PARP Inhibitors

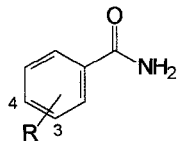

Code	R	IC_{50}(μM) [a]
1 Benzamide	H	22.0
2	3-F	20.0
3	4-F	200
4	3-Cl	22.0
5	4-Cl	300
6	3-NH_2	33.0
7	4- NH_2	1800
8	3-Br	55
9	4-Br	2200
10	3-OCH_3	17.0
11	3-OH	9.10
12	4-OH	280
13	3-CH3	19.0
14	3-NO_2	160
15	3-$N(CH_3)_2$	120

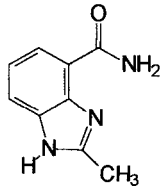

Code	IC_{50}(μM) [c]
16 NU1064	1.00

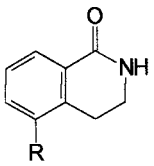

Code	R	IC_{50}(μM)
17 PD128763	CH_3	0.44 [b]
18 DPQ	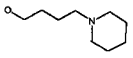	0.04 [d]

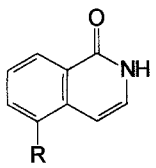

Code	R	IC_{50}(μM) [a]
19	H	7.00
20 DHQ	OH	0.39

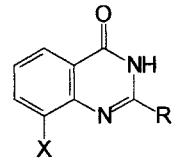

Code	R	X	IC_{50}(μM) [a]
21	H	H	9.50
22	CH_3	H	5.60
23 NU1025	CH_3	OH	0.40 [b]

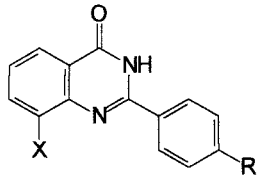

Code	R	X	IC_{50}(μM) [b]
24	H	CH_3	0.87
25	H	OCH_3	4.2
26	NO_2	CH_3	0.13
27	NO_2	OCH_3	0.85
28	CF_3	OCH_3	39
29	CN	CH_3	0.27
30	CN	OCH_3	1.34
31	OCH_3	CH_3	0.19
32	OCH_3	OCH_3	2.0
33	NH_2	CH_3	0.44
34	CO_2CH_3	CH_3	4.80
35	H	OH	1.06
36	NO_2	OH	0.23
37	OH	OH	0.29
38	OH	CH_3	0.22
39	NH_2	OH	0.52

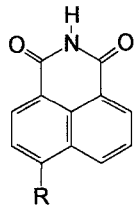

Code	R	IC_{50}(μM) [a]
40	H	1.40
41	NH_2	0.18

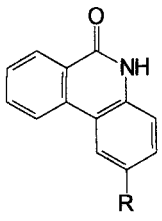

Code	R	IC_{50}(μM) [a]
42 PTD	H	0.30
43	NO_2	0.35

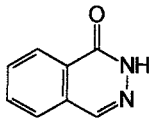

Code	IC_{50}(μM) [a]
44 1(2*H*)-Phthalazinone	12

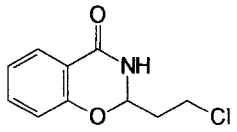

Code	IC_{50}(μM) [a]
45 Chlorthenoxazin	8.5

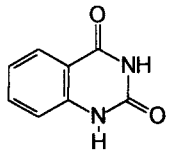

Code	IC_{50}(μM) [a]
46 Benzoylenurea	8.1

[a] Reference 16. [b] Reference 18. [c] Reference 29. [d] Reference 9.

rity of properties with the model. A solvation correction term and the electrostatic charge complementarity method were used for energy evaluation. The solvation energy correction term is a penalty function that attempts to account for the

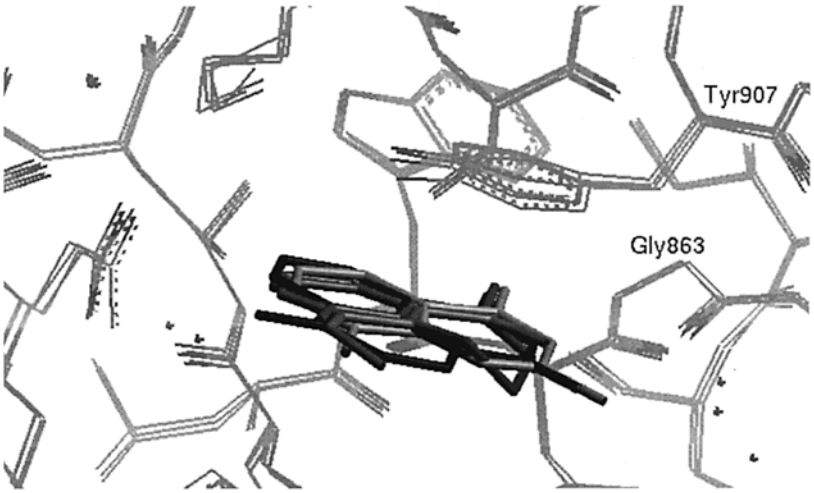

Figure 1. Superposition of the catalytic sites of crystallized complexes of PARP (1pax, 2pax, 3pax, 4pax) with some inhibitors. Binding pocket residues are displayed in thin lines, while inhibitors are shown in thick lines. Key residues are evidenced.

loss of solvation when polar atoms are forced into hydrophobic regions of the receptor surface.

The correlation between the inhibitory activity (dependent variable), expressed as $\ln(1/IC_{50})$, and a series of molecular descriptors related to the binding energy was quantitatively studied by means of multiple linear regression analysis. A cross-validation protocol and randomization test were used to determine the statistical significance of the analyses. The predictive index of the generated models is given by the cross-validated r^2 (r^2_{cv}, q^2). All of the regression analyses were performed on autoscaled variables. Outliers, if present, were removed, and new analyses were carried out. All calculations were carried out on a SGI O2 R5500 machine using the QSAR module implemented in the Cerius2 software package distributed by Molecular Simulations Inc.[27]

Results and Discussion

The RECEPTOR approach consists of creating receptor surface models that characterize the spatial and electrostatic properties of the active site of an enzyme or a receptor on the basis of a starting alignment of a set of active compounds. The interaction energies between these surfaces and the set of compounds are calculated and transformed into molecular descriptors, which can be used to quantitatively study the dependence of the biological activity on them. An underlying complementarity is assumed between the shape and properties of the receptor and the set of compounds that bind to it. Crucial to the success of the procedure is the choice of a correct alignment scheme for the chosen inhibitors. The alignment of the 46 inhibitors (Table 1) was constructed in two steps. In the first step, docking experiments were carried out on a small subset of compounds to obtain information on the binding geometry of structurally diverse compounds. In the second step, the remaining compounds were aligned by fitting the coordinates of common interaction points that resulted from docked inhibitors.

Docking Results. Four compounds [DPQ (**18**), 4-amino-1,8-naphthalimide (**41**), 6(*5H*)-phenanthridinone (**42**), and 8-methyl 2-(4′-nitrophenyl)quinazolin-4-one (**26**)] were selected from the starting set of 46 compounds and subjected to docking experiments. The automated docking procedure of Autodock 2.4 was used for this aim. The atomic coordinates of the catalytic domain of PARP were retrieved from the Protein Data Bank (PDB) database. Several PARP structures were in fact present. Some of them are crystallographic structures of the catalytic domain of the unbound enzyme, while others are structures of the enzyme cocrystallyzed with competitive inhibitors. Visual inspection and superimposition of these structures revealed that no significant differences at the level of the backbone atoms occur between the bound and the unbound enzyme (rms < 0.5 Å). Thus, we decided to take the unbound structure of PARP as the reference structure (PDB code: 2paw). The chosen parametrization of Autodock (see Methods) was tested for its ability to reproduce the crystallized binding geometry of 3,4-dihydro-5-methylisoquinolinone (**17**, PDB code: 1pax) and 4-amino-1,8-naphthalimide (**41**, PDB code: 2pax) into the unbound catalytic site of PARP (PDB code: 2paw). In both cases, Autodock easily found the binding geometry corresponding to the crystallized complex among the solutions with the lowest energy, being the rms deviation between the docked and the crystallized geometry in the limit of the crystallographic resolution (rms < 1.0 Å, resolution > 2.0 Å, Table 2). It should be noticed that, because the rms deviation is evaluated over all of the heavy atoms of the protein and the ligand, the goodness of the reproducibility of the ligand position can be overestimated. Thus, we added other parameters, namely, the distances between the amido moiety of the inhibitors and Gly863 (columns 6 and 7, Table 2), as indicators of the goodness of the fit. This criterion clearly applies for compounds **18**, **26**, and **42** (Table 2), for which no crystallized references are available.

Thus, compounds **18**, **26**, **41**, and **42** were subjected to docking experiments and shown to bind the catalytic domain of PARP with "conserved" and "unconserved" interactions (Table 2 and Figure 2). Conserved interactions are those displayed by all the studied compounds and include hydrogen bonds between the amide moiety and the backbone of Gly863, and $\pi-\pi$ interactions between the aromatic group of the inhibitors and the side chain of Tyr907. Nonconserved interactions are strictly dependent on the structural diversity of docked inhibitors. Thus, while DPQ (**18**) forms a salt bridge interaction with Asp766 (Figure 2a), the amino group of 4-amino-1,8-naphthalimide (**41**) forms additional hydrogen bonds with Glu988 (Figure 2b), and the nitro

Table 2

structure	rank	ΔE_{rank} (kcal/mol)	cluster	rmsd[a]	distance (Å)[b] (NGly−OAmd)	distance (Å)[b] (OGly−NAmd)
17[c]	1	0.00	1/10	0.51	7.56	4.07
	2	0.04	1/10	0.55	8.26	8.50
	3	*0.07*	*6/10*	*0.46*	*2.65*	*2.78*
	4	0.32	2/10	0.52	6.52	5.93
41[c]	1	0.00	5/10	8.25	8.62	9.18
	2	0.33	1/10	8.24	8.51	9.05
	3	*0.71*	*4/10*	*0.46*	*2.89*	*3.01*
18	*1*	*0.00*	*1/10*		*2.97*	*2.75*
	2	0.08	1/10		2.97	2.81
	3	0.36	3/10		2.94	2.75
	4	1.53	3/10		12.19	8.00
	5	3.41	1/10		12.55	9.17
	6	3.97	1/10		7.59	7.98
26	*1*	*0.00*	*5/10*		*2.67*	*2.94*
	2	0.09	3/10		2.81	2.87
	3	0.57	1/10		3.09	2.99
	4	0.96	1/10		5.18	5.35
42	*1*	*0.00*	*10/10*		*2.95*	*2.86*

[a] Calculated between the solutions of Autodock in the unbound enzyme (PDB code: 2paw) and the crystal complex of **17** and **41** (PDB codes: 1pax, 2pax) by fitting all heavy atoms. The solutions, marked in italic, of compounds **18**, **26**, **41**, and **42** were chosen to construct the starting alignment. [b] Distances between the amido group of the docked ligands and N−O atoms of Gly863. [c] Compounds used to validate the computational protocol of Autodock (see text for details).

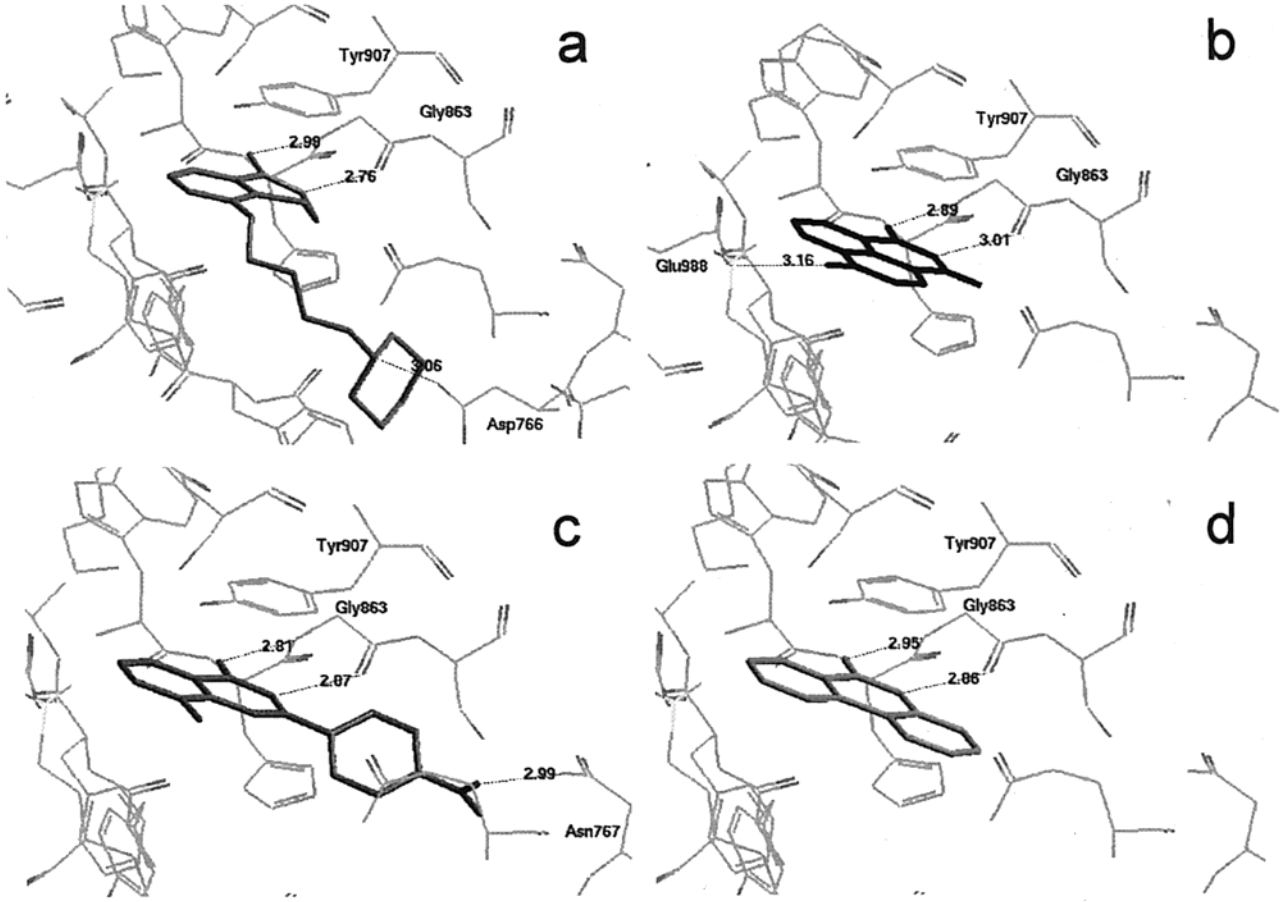

Figure 2. Results of docking experiments of DPQ (**18,** a), **41** (b), **26** (c), and **42** (d) into the catalytic site of PARP. Conserved and unconserved interactions are evidenced.

group of 8-methyl 2-(4′-nitrophenyl)quinazolin-4-one (**26**) forms hydrogen bonds with the side chain of Asn767 (Figure 2c).

Conserved and nonconserved (where possible) interaction points were used as reference coordinates to align the remaining 42 compounds of the starting set. More in detail, the alignment scheme is reproduced in Figure 3, in which the three conserved reference points (amido moiety and the centroid of the aromatic ring) are highlighted. The underlying assumption of this alignment scheme is that all of the undocked compounds are supposed to be positioned in the binding pocket in a orientation identical to that of one of the four referenced compounds on the basis of their structural relationship.

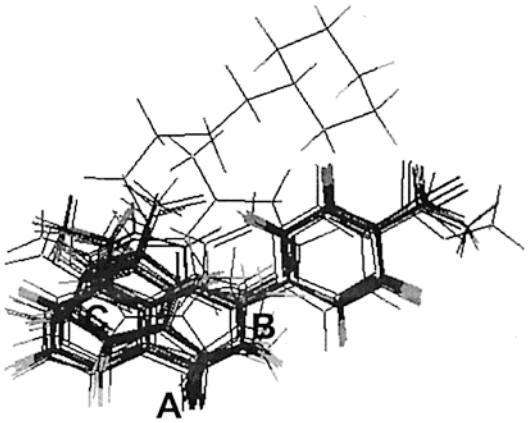

Figure 3. Alignment scheme. The conserved reference points are marked as A, B (amido moiety), and C (aromatic centroid).

Generation of Surface Models. To build a surface model of the binding cavity of PARP, a subset of eight compounds (**16**, **18**, **26**, **29**, **31**, and **41**−**43**) was selected from the initial set of molecules (Table 1). The rationale behind the choice of this subset of molecules was to take into account as much molecular diversity as possible and a broad range of inhibitory potencies, in such a way to efficiently train the model. Surface models were generated using the RECEPTOR approach, as described in the Methods. All 46 compounds of the starting set were then energetically evaluated inside the surface model of the catalytic site of PARP. In particular, two energetic descriptors were calculated: the van der Waals energy of interaction (E_{VdW}) and the electrostatic energy of interaction (E_{elec}). Moreover, three other descriptors were computed: the number of hydrogen-bond-donating groups (H_{don}), the number of hydrogen-bond-acceptor groups (H_{acc}), and the number of torsional angles (N_{tors}). All of the above descriptors (data available as Supporting Information) are related to the enthalpy and entropy of binding.

QSAR Analysis. The dependence of the inhibitor activity on these descriptors was quantitatively studied by means of multiple linear regression analysis (Table 3). A starting run using 46 objects and 5 variables was performed. The result yields a r^2 of 0.656 and a predictive q^2 of 0.564. Four compounds (**7**, **9**, **20**, and **23**) are poorly predicted. In particular, **7** and **9** are predicted to be more active than they are, while **20** and **23** are predicted to be less active than they are. The inspection of the compound's structures did not reveal any immediate reasons for their bad prediction, although it should be noticed that compound **9** is present in the literature with discordant values of inhibitor activity (IC_{50} = 400 μM, IC_{50} = 1800 μM).[16,30] To gain more insights into the origin of these bad predictions, the four outliers were subjected to docking experiments using the above-described protocol. The results are summarized in Table 4. In particular, for compounds **7** and **9**, we were unable to find a docking orientation compatible with the chosen alignment scheme among the top-ranked solutions. This is apparently due to the presence of the substituent (amino and bromine, respectively) in the 4-position, which makes very unfavorable contacts with Glu988. The weak activity of compounds **7** and **9** must therefore be ascribed to a poorly productive orientation into the binding pocket, an effect that is difficult to reproduce in an alignment scheme. Indeed, a close examination of Table 4 shows that the second solution for compound **7** could be correct in terms of distances to Glu863. However, the second solution in Table 4 has only a $^1/_{10}$ occurrence, and furthermore, even if the second docking solution is correct, compound **7** has a 4-substituent (see Table 1). Lack of the predictivity can partially be attributed to steric effects of the 4-substituents observed in the series. As far as compounds **20** and **23** are concerned, they are fairly well-positioned in the binding pocket by the docking algorithm. Thus, their superimposition to the alignment scheme cannot be considered as a cause for their bad prediction. This is further confirmed by the observation that the X-ray structure of compound **23** complexed with PARP is available (PDB code: 4pax): the top-ranked docking result reproduces the experimental orientation. Because **20** and **23** are predicted to be less active than they are, there could be a specific effect of the hydroxy substituent in the 5-position. However, the examination of the X-ray structure of 4pax reveals that the hydroxy group is not involved in any specific interaction (Figure 4).

Thus, the effect of the hydroxy group should be either due to a water bridge (not visible in the X-ray structure) or due to a more subtle effect, such as a lowering of the LUMO energy of the aromatic ring and an increase in the $\pi-\pi$ interaction with Tyr907. Taken together, these considerations seem to indicate that very specific effects play a role for compounds **7**, **9**, **20**, and **23**, which can therefore be considered as outliers. The four outliers were removed, and the analysis was carried out again yielding a r^2 = 0.804 and q^2 = 0.738 (Figure 5). This model was validated by means of some tests, including leave-one-out cross-validation, randomization tests, and external predictions on a limited test set. This test set was created by splitting the original set into two parts, a training set of 38 compounds and test set of 4 compounds, chosen on the basis of their structural and biological diversity. The results, summarized in Table 3, indicate the reliability of the model.

Table 3

	run 1	run 2
r^2	0.656	0.804
q^2	0.564	0.738
F test	15.290	29.556
bootstrap r^2	0.657	0.805
bootstrap r^2 error	0.006	0.002
no. objects	46	42
no. indep variables	5	5
outliers	4 (**7**, **9**, **20**, **23**)	-
PRESS	138.867	60.266
mean	−1.438	−1.258
SD	318.808	230.383

confidence level, 99%
mean value of r from random trials, 0.341 979
standard deviation of random trials, 0.099 874
standard deviation from nonrandom r to mean, 5.554 430

External Prediction on an External Test Set Composed of Four Compounds
No. Obj = 38; r^2 = 0.795; q^2 = 0.720; F test = 24.853

structure	ln 1/IC_{50} (μM)	predicted	residual
15	−4.78	−3.40	−1.38
16	0.00	−0.64	0.64
31	1.66	1.55	0.11
44	−2.48	−1.49	−0.99

Table 4

structure	rank	ΔE_{rank} (kcal/mol)	cluster	rmsd[a]	distance (Å)[b] (NGly−OAmd)	distance (Å)[b] (OGly−NAmd)
7	1	0.00	9/10		9.80	9.26
	2	0.58	1/10		2.66	2.61
9	1	0.00	4/10		9.52	9.63
	2	0.07	1/10		4.69	4.90
	3	0.18	4/10		5.25	5.32
	4	0.25	1/10		14.84	11.92
20	1	0.00	6/10		8.08	8.06
	2	0.20	2/10		2.67	3.08
	3	0.29	1/10		3.11	2.75
	4	0.33	1/10		4.54	3.56
23	1	0.00	8/10	0.52	3.03	2.92
	2	0.65	1/10	7.72	7.96	5.17
	3	0.81	1/10	7.73	2.69	5.89

[a] Calculated between the solution of Autodock in the unbound enzyme (PDB code: 2paw) and the crystal complex of **23** (PDB code: 4pax) by fitting all the heavy atoms. [b] Distances between the amido group of the docked ligands and N−O atoms of Gly863.

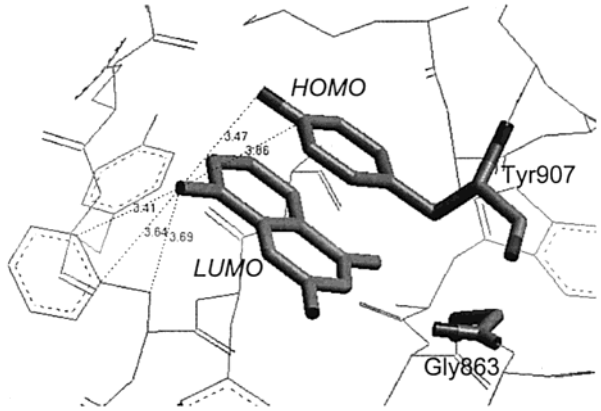

Figure 4. X-ray structure of compound **23** in the binding site of PARP (4pax). Dashed lines represent distances between enzyme functional groups and the 5-hydroxy of the inhibitor.

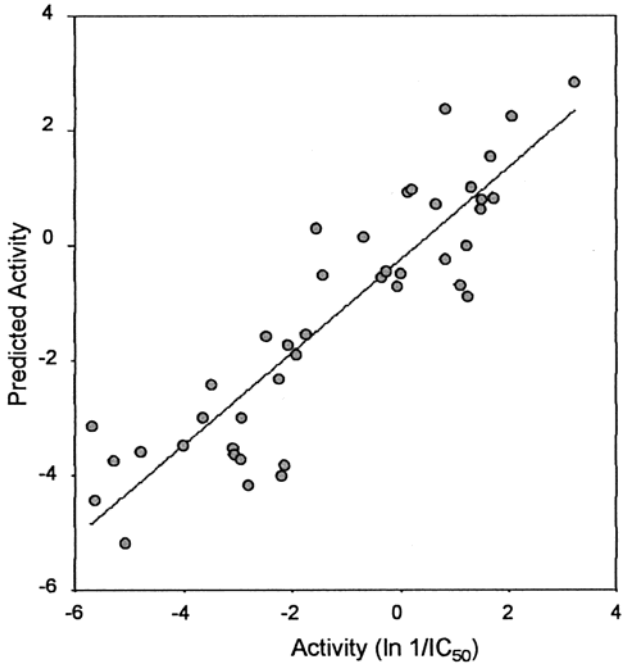

Figure 5. Plot of observed versus predicted activity.

The regression coefficients of the QSAR equation (eq 2) give the qualitative and quantitative influence of each descriptor in determining the inhibitor activity. The high coefficient of the van der Waals energy descriptor can be appreciated, while the effects of the other descriptors are less important although not negligible. The positive influence of the van der Waals interaction energy means that the more extensive is the surface in contact between the molecule and the catalytic site of PARP, the more potent is the inhibitor activity of the molecule. In contrast, the number of torsional angles (N_{tors}) plays the opposite effect because of entropic factors. As an example, the high activity of compound **18** can be related to the high van der Waals contacts of the butoxy-piperidinyl chain with the enzyme. Compound **17**, however, in which a methyl group substitutes for the butoxy-piperidinyl chain, is only slightly weaker in potency than **18**, an effect that can be ascribed to the high number of N_{tors} of **18**.

$$y = -9.56 - 0.37E_{elec} - 2.93E_{VdW} - 0.96N_{tors} - 0.24H_{acc} + 0.46H_{don}$$

The projection of the coefficient maps into the crystallized structure of the catalytic domain of PARP permits giving structural bases to the quantitative correlation. Thus, van der Waals interaction energies were mapped on the surface model of the binding site for representative compounds such as DPQ (**18**, $IC_{50} = 0.04\ \mu M$), **28** ($IC_{50} = 39\ \mu M$), **27** ($IC_{50} = 0.85\ \mu M$), **32** ($IC_{50} = 2.0\ \mu M$), and **6** ($IC_{50} = 33\ \mu M$) (Figure 6).

The maps indicate favorable (magenta) and unfavorable (green) interactions. In contrast to compound **6**, DPQ (**18**) presents a wide region of favorable interactions with only a small "green" portion near the second methylene group of the side chain (Figure 6b and 6a, respectively). 3-Aminobenzamide (**6**), which has an IC_{50} of 33 μM, fits neatly the binding pocket and has a correct interaction geometry between the amide moiety and Gly863 and between the aromatic ring and Tyr907. The low value of activity must therefore be ascribed to the small region of contact with the binding pocket of the enzyme. More intriguing is the behavior of compounds **27**, **28**, and **32**. Compound **28** has the lowest activity among the series of 2-(4′-substituted-phenyl)-8-substituted quinazolines, while **27** and **32** are significantly potent, the only difference being the substitution of a trifluoromethyl moiety (in **28**) by a nitro (**27**) or a methoxy group (**32**). Inspection of the maps reveals that the lower activity of **28** can be attributed to regions of unfavorable van der Waals interactions present above and below the trifluoromethyl moiety (Figure 6c), while the planar nitro group (Figure 6d) and the methoxy

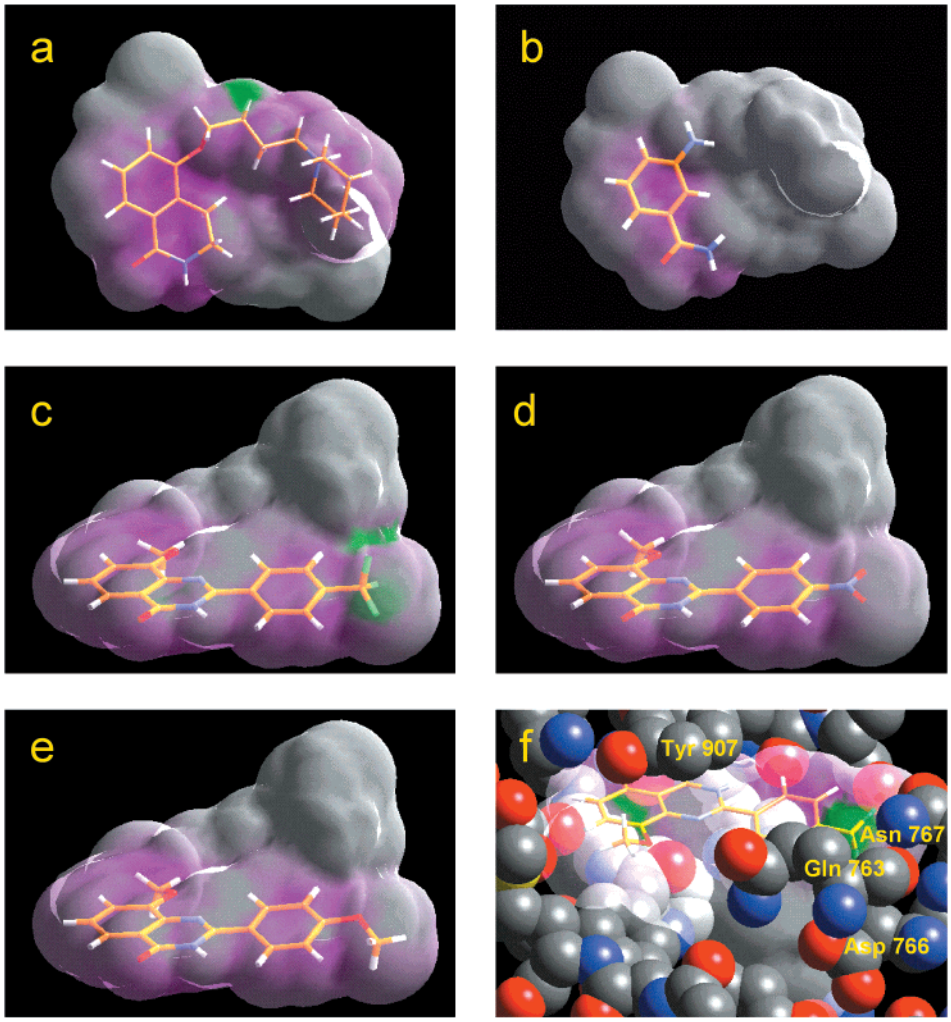

Figure 6. Favorable (magenta) and unfavorable (green) van der Waals interactions for **18** (a), **6** (b), **28** (c), **27** (d), and **32** (e) and plot of surface maps of compound **28** in the catalytic site of PARP (f). See text for details.

group (Figure 6e) can be accommodated without significant bumps with the receptor. When plotted into the binding site of PARP, these regions are localized near Asn767, Asp766, Gln763, and the hydroxy group of Tyr907 (Figure 6f).

In conclusion, and quite unexpectedly, the major determinant for high inhibitory potency seems to be given by the extension of the contact surfaces between inhibitors and enzyme, although the presence of hydrogen-bond-forming groups can increase the affinity within a homogeneous series of compounds (e.g., **18** in the series of dehydroisoquiloninones or **41** in the series of 1,8-naphthalimide). Besides this general trend, however, more subtle effects cooperate in determining the potency of individual inhibitors, as exemplified by the series of (4′-substituted-phenyl)-8-substituted quinazolines (**27**−**32**, Table 1) or by the very peculiar behavior of compounds **20** and **23**. The inspection of the binding mode of selected classes of PARP inhibitors, either by docking experiments or by examination of the QSAR equations, has allowed us to put forward some of the structural features that may affect the binding of inhibitors, indications that can be instrumental in the design of novel derivatives.

Conclusion

The combined approach of docking studies and QSAR analysis allowed us to gain insights into the structural basis of PARP-1 inhibition. From a methodological point of view, the combined docking/QSAR approach, which has successful precedents,[26,27] seems to be a generally sound methodology which allows one to merge the experimentally derived information from docking to crystallographically determined structure with the computational power of ligand-based design and quantitative structure−activity relationships. In our particular case, the Autodock 2.4 algorithm was shown to be able to reproduce the experimentally observed mode of binding of representative PARP inhibitors, thus demonstrating a suitable approach for virtually screening new potential inhibitors. In addition, the alignment scheme deduced from the docking experiments was instrumental in defining a predictive QSAR model that can be used for prioritizing a list of potential inhibitors to be synthesized. In conclusion, the results here reported can usefully be employed for the rational design of novel, potent PARP-1 inhibitors in the search for novel neuroprotective agents.

Acknowledgment. Financial support from Smith Kline Beecham (U.K.) is gratefully acknowledged.

Supporting Information Available: A table of data from the surface model calculations. This material is available free of charge via the Internet at http://pubs.acs.org.

References

(1) Ha, H. C.; Snyder, S. H. Poly(ADP-ribose) polymerase-1 in the nervous system. *Neurobiol. Dis*. **2000**, *7*, 225−239.
(2) De Murcia, G.; Schreiber, V.; Molinete, M.; Saulier, B.; Poch, O.; Masson, M.; Niedergang, C.; Menissier de Murcia, J. Structure and function of poly(ADP-ribose) polymerase. *Mol. Cell. Biochem*. **1994**, *138*, 15−24.
(3) Griffin, R. J.; Curtin, N. J.; Newell, D. R.; Golding, B. T.; Durkacz, B. W.; Calvert, A. H. The role of inhibitors of poly-(ADP-ribose) polymerase as resistance-modifying agents in cancer therapy. *Biochimie* **1995**, *77*, 408−422.
(4) Shall, S.; De Murcia, G. Poly(ADP-ribose) polymerase-1: what have we learned from the deficient mouse model? *Mutat. Res*. **2000**, *460*, 1−15.
(5) Plaschke, K.; Kopitz, J.; Weigand, M. A.; Martin, E.; Bardenheuer, H. J. The neuroprotective effect of cerebral poly(ADP-ribose)polymerase inhibition in a rat model of global ischemia. *Neurosci. Lett*. **2000**, *284*, 109−112.
(6) Takahashi, K.; Greenberg, J. H. The effect of reperfusion on neuroprotection using an inhibitor of poly(ADP-ribose) polymerase. *NeuroReport* **1999**, *10*, 2017−2022.
(7) Szabo, C.; Dawson, V. L. Role of poly(ADP-ribose) synthetase in inflammation and ischaemia-reperfusion. *Trends Pharmacol. Sci*. **1998**, *19*, 287−298.
(8) Endres, M.; Wang, Z. Q.; Namura, S.; Waeber, C.; Moskowitz, M. A. Ischemic brain injury is mediated by the activation of poly-(ADP-ribose)polymerase. *J. Cereb. Blood Flow Metab*. **1997**, *17*, 1143−1151.
(9) Eliasson, M. J.; Sampei, K.; Mandir, A. S.; Hurn, P. D.; Traystman, R. J.; Bao, J.; Pieper, A.; Wang, Z. Q.; Dawson, T. M.; Snyder, S. H.; Dawson, V. L. Poly(ADP-ribose) polymerase gene disruption renders mice resistant to cerebral ischemia. *Nat. Med*. **1997**, *3*, 1089−1095.
(10) Brauner-Osborne, H.; Egebjerg, J.; Nielsen, E. O.; Madsen, U.; Krogsgaard-Larsen, P. Ligands for glutamate receptors: design and therapeutic prospects. *J. Med. Chem*. **2000**, *43*, 2609−2645.
(11) Obrenovitch, T. P.; Urenjak, J.; Zilkha, E.; Jay, T. M. Excitotoxicity in neurological disorders—the glutamate paradox. *Int. J. Dev. Neurosci*. **2000**, *18*, 281−287.
(12) Pieper, A. A.; Verma, A.; Zhang, J.; Snyder, S. H. Poly (ADP-ribose) polymerase, nitric oxide and cell death. *Trends Pharmacol. Sci*. **1999**, *20*, 171−181.
(13) Takahashi, K.; Pieper, A. A.; Croul, S. E.; Zhang, J.; Snyder, S. H.; Greenberg, J. H. Posttreatment with an inhibitor of poly-(ADP-ribose) polymerase attenuates cerebral damage infocal ischemia. *Brain Res*. **1999**, *829*, 46−54.
(14) Plaschke, K.; Kopitz, J.; Weigand, M. A.; Martin, E.; Bardenheuer, H. J. The neuroprotective effect of cerebral poly(ADP-ribose)polymerase inhibition in a rat model of global ischemia. *Neurosci. Lett*. **2000**, *284*, 109−112.
(15) Lo, E. H.; Bosque-Hamilton, P.; Meng, W. Inhibition of poly-(ADP-ribose) polymerase: reduction of ischemic injury and attenuation of *N*-methyl-D-aspartate-induced neurotransmitter dysregulation. *Stroke* **1998**, *29*, 830−836.
(16) Banasik, M.; Komura, H.; Shimoyama, M.; Ueda, K. Specific inhibitors of poly(ADP-ribose) synthetase and mono(ADP-ribosyl)transferase. *J. Biol. Chem*. **1992**, *267*, 1569−1575.
(17) Suto, M. J.; Turner, W. R.; Arundel-Suto, C. M.; Werbel, L. M.; Sebolt-Leopold, J. S. Dihydroisoquinolinones: the design and synthesis of a new series of potent inhibitors of poly(ADP-ribose) polymerase. *Anti-Cancer Drug Des*. **1991**, *6*, 107−117.
(18) Griffin, R. J.; Srinivasan, S.; Bowman, K.; Calvert, A. H.; Curtin, N. J.; Newell, D. R.; Pemberton, L. C.; Golding, B. T. Resistance-modifying agents. 5. Synthesis and biological properties of quinazolinone inhibitors of the DNA repair enzyme poly(ADP-ribose) polymerase (PARP). *J. Med. Chem*. **1998**, *41*, 5247−5256.
(19) White, A. W.; Almassy, R.; Calvert, A. H.; Curtin, N. J.; Griffin, R. J.; Hostomsky, Z.; Maegley, K.; Newell, D. R.; Srinivasan, S.; Golding, B. T. Resistance-Modifying Agents. 9. Synthesis and Biological Properties of Benzimidazole Inhibitors of the DNA Repair Enzyme Poly(ADP-ribose) Polymerase *J. Med. Chem*. **2000**, *43*, 4084−4097.
(20) Ruf, A.; Mennissier de Murcia, J.; De Murcia, G.; Schulz, G. E. Structure of the catalytic fragment of poly(ADP-ribose) polymerase from chicken. *Proc Natl Acad Sci U.S.A*. **1996**, *93*, 7481−7485.
(21) Ruf, A.; De Murcia, G.; Schulz, G. E. Inhibitor and NAD+ binding to poly(ADP-ribose) polymerase as derived from crystal structures and homology modeling. *Biochemistry* **1998**, *37*, 3893−3900.
(22) Jung, S.; Miranda, E. A.; De Murcia, J. M.; Niedergang, C.; Delarue, M.; Schulz, G. E.; De Murcia, G. M. Crystallization and X-ray crystallographic analysis of recombinant chicken poly-(ADP-ribose) polymerase catalytic domain produced in Sf9 insect cells. *J. Mol. Biol*. **1994**, *244*, 114−116.
(23) Hagler, A. T.; Huler, E.; Lifson, S. Energy Functions for Peptides and Proteins. I. Derivation of a Consistent Force Field Including the Hydrogen Bond from the Amide Crystals. *J. Am. Chem. Soc*. **1974**, *96*, 5319−5327.
(24) Morris, G. M.; Goodsell, D. S.; Huey, R.; Olson, A. J. Distributed automated docking of flexible ligands to proteins: parallel applications of AutoDock 2.4. *J. Comput.-Aided Mol. Des*. **1996**, *10*, 293−304.
(25) Hahn, M. Receptor surface models. 1. Definition and construction. *J. Med. Chem*. **1995**, *38*, 2080−2090.
(26) Hahn. M.; Rogers, D. Receptor surface models. 2. Application to quantitative structure−activity relationships studies. *J. Med. Chem*. **1995**, *38*, 2091−2102.
(27) Sippl, W. Receptor-based 3D QSAR analysis of estrogen receptor ligands—merging the accuracy of receptor-based alignments with the computational efficiency of ligand-based methods. *J. Comput.-Aided Mol. Des*. **2000**, *14*, 559−572.
(28) Lozano, J. J.; Pastor, M.; Cruciani, G.; Gaedt, K.; Centeno, N. B.; Gago, F.; Sanz, F. 3D-QSAR methods on the basis of ligand−receptor complexes. Application of COMBINE and GRID/GOLPE methodologies to a series of CYP1A2 ligands. *J. Comput.-Aided Mol. Des*. **2000**, *14*, 341−353.
(29) Bowman, K. J.; White, A.; Golding, B. T.; Griffin, R. J.; Curtin, N. J. Potentiation of anti-cancer agent cytotoxicity by the potent poly(ADP− ribose) polymerase inhibitors NU1025 and NU1064. *Br. J. Cancer* **1998**, *78*, 1269−1277.
(30) Rankin, P. W.; Jacobson, E. L.; Benjamin, R. C.; Moss, J.; Jacobson, M. K.; Quantitative studies of inhibitors of ADP-ribosylation in vitro and in vivo. *J. Biol. Chem*. **1989**, *264*, 4312−4317.

JM010116L